ELSEVIER

Catalysis Communications 3 (2002) 239–245

CATALYSIS COMMUNICATIONS

www.elsevier.com/locate/catcom

A comparison of surface acidic features between tetragonal and monoclinic nanostructured zirconia

Yubao Zhao, Wei Li, Minghui Zhang, Keyi Tao *

Institute of New Catalytic Materials Science, Nankai University Tianjin 300071, China

Received 21 January 2002; received in revised form 27 March 2002; accepted 27 March 2002

Abstract

Systematic analysis about the difference of surface acidic features between tetragonal and monoclinic nanostructured zirconia is presented. Unlike the monoclinic zirconia, both Brønsted acid sites and Lewis acid sites exist on its surface, only Lewis acid sites measurable by IR spectroscopy after pyridine adsorption are found on tetragonal zirconia. There exists a parallel relationship between Zr^{4+} density and the surface acid-site density for tetragonal and monoclinic zirconia. The surface Zr^{4+} densities of tetragonal and monoclinic zirconia derived from their preferential planes are approximately 3 times their surface acid-site densities determined by NH_3-adsorption measurements. © 2002 Published by Elsevier Science B.V.

Keywords: Nanostructured; Zirconia; Monoclinic; Tetragonal; Acid features; Preferential planes

1. Introduction

Due to the amphoteric and promising property [1], zirconia has received considerable attention both as a catalyst and as a catalyst support [2–9]. The crystal structure of zirconia is well known. Less well known is its influence on the catalytic performance of zirconia-based catalysts. In 1979, Tanabe et al. [1] have found that ZrO_2 evaluated at 873 K shows a maximum activity for the hydrogenation of 1,3-butadiene with hydrogen, whereas ZrO_2 evaluated at 1073 K gives the maximum activity for the hydrogenation of cyclohexadiene. They intended to take the lattice-constant change of ZrO_2 with the change of calcination temperature as the explanation of the observed activity difference. Study on the catalytic performance of zirconia for CO hydrogenation shows that monoclinic zirconia (MZ) has high selectivity to butene, while on tetragonal zirconia (TZ) the main products are methane, ethene, propene [10]. Yori and Parera reported that the larger the fraction of the tetragonal phase of zirconia in Pt/WO_3-ZrO_2, the higher the activity of *n*-butane isomerization and the lower the metallic activity of Pt [11]. Very recently Stichert et al. [12] observed the activity of monoclinic sulfate zirconia is lower by a factor of 2–5 compared to tetragonal sulfated zirconia for *n*-butane isomerization in a fixed-bed flow reactor at

* Corresponding author. Tel.: +86-22-23500027; fax: +86-22-23500027.

E-mail address: kytao@nankai.edu.cn (K. Tao).

1566-7367/02/$ - see front matter © 2002 Published by Elsevier Science B.V.
PII: S1566-7367(02)00089-4

573 K. Their finding is in accord with our experimental result in a static reactor at 313 K [13].

As the reaction catalyzed by solid catalysts is a surface process, efforts should be directed to the surface structures and surface properties of solid catalysts to understand their catalysis. Its well known coordination environments of zirconium and oxygen in zirconia polymorphs are apparently different. In the tetragonal lattice the Zr^{4+} cation is octacoordinated and the O^{2-} anion is tetracoordinated. Whereas in the monoclinic lattice the Zr^{4+} cation is heptacoordinated and the O^{2-} anion is either tri- or tetracoordinated [14]. This significant structural difference makes one expect that there probably exist some surface-feature differences between TZ and MZ. In this paper, we compared the Zr^{4+} densities in (1 1 1) and (1 0 1) planes of TZ as well as the Zr^{4+} densities in (1 1 1) and ($\bar{1}$ 1 1) planes of MZ with the experimental acid-site densities.

2. Experimental

2.1. Sample preparation

Monoclinic zirconia was prepared by a reflux-hydrolysis route. A 0.4 mol dm^{-3} aqueous solution of $ZrOCl_2$ was digested under open reflux at a slightly boiling state for a time no more than 96 h. Then ammonia was added to the resulting sol until pH 9.3 was reached. The precipitate was washed till the negative test for chloride, separated, dried overnight at 383 K, and finally calcined in air at 773 K for 4 h. The as-prepared samples were denoted as MZx, where x represents the refluxing time in hours. Tetragonal zirconia was prepared by 50 h refluxing the fresh precipitate from $ZrOCl_2$ and ammonia solution at pH of 9.3. After washed, separated and dried, the solid was calcinated in air at 873 K for 4 h and referred to as TZ50. Here the adoption of 873 K is necessary to obtain the tetragonal zirconia because the as-prepared ZrO_2 calcinated at 773 K is still amorphous.

2.2. Characterization

The specific surface area measurements were carried out at 77 K with a Coulter-Omnisorp™ Model 100 automatic system. TEM observation was performed with a Philips EM400ST microscopy. The XRD patterns were obtained with a D/MAX-2500 diffractometer (Rigaku, Japan) using CuKα radiation. The average thickness of a coherently diffracting domain in the direction perpendicular to the (1 1 1) plane for tetragonal phase or to the ($\bar{1}$ 1 1) plane for monoclinic phase, was calculated using the well known Scherrer equation. Laser Raman spectra (LRS) were recorded using a Bruker RFS 100/S spectrometer at a resolution of 2 cm^{-1} and scanning 100 times.

IR spectra were registered with a Bruker VECTOR 22 FTIR spectrometer. Self-supporting pellets (15–20 mg/cm^2) were activated in situ at 673 K (2 h). After exposed to pyridine vapor at ambient temperature for 30 min, the wafers were outgassed at 423 K for 1 h and then IR spectra were collected at room temperature with a resolution of 2 cm^{-1}. Both Brønsted and Lewis acid-site densities were calculated by the following equation [15]:

$$n_i = \frac{A_i a_c}{\varepsilon_i m}, \tag{1}$$

where n_i is the amount of type i acid sites in microtnoles per gram, A_i the integrated absorbance in cm^{-1}, a_c the cross-sectional area in square centimeters of the wafer, ε_i the integrated molar extinction coefficient in cm μmol^{-1} and m the mass of sample in grams.

NH_3 chemisorption was evaluated by a volumetric method. After treated in dynamic vacuum (<10 Pa) at 773 K for 1 h, a 150 mg sample was exposed to a 10 kPa ammonia vapor at 393 K for 30 min. Thus the total NH_3 adsorption amount (n_t) can be calculated from the predetermined volumes and the pressure change during the adsorption process. Then the sample was evacuated at 393 K for another 30 minutes to eliminate the physisorption at this temperature. The next step was to determine the physical-adsorption amount (n_p) by contacting the sample with ammonia once more in the same conditions. Thus the NH_3 chemisorption amount (n_c) can be calculated using the equation $n_c = n_t - n_p$. Considering at low temperature physisorption often overweights chemisorption and generally only the chemisorp-

Table 1
Specific surface areas from XRD and BET measurements of TZ50 and MZ96

Sample	S_{XRD} (m^2 g^{-1})	S_{BET} (m^2 g^{-1})
TZ50	131	120
MZ96	94	65

tion is important to catalysis, we performed our experiments at 393 K to minimize the physical adsorption and experimentally subtracted its effect at this temperature. In fact, the NH_3-TPD profiles (not shown here) for these samples after the final physisorption-eliminated treatment show that the temperature, at which ammonia begins to desorb, is over 413 K. This means that the final treatment can vacuum out all the physically adsorbed ammonia molecule. As ammonia desorbs quickly when temperature is over 423 K (TPD results), the ammonia chemisorption amount of zirconia determined at temperature higher than 423 K will be lower than its real value.

3. Results and discussion

3.1. Identification of crystal phase

The XRD patterns of MZ*x* (Fig. 1) show that their crystal phase is monoclinic (JCPDS No. 37-1484). And an average crystallite size of 11 nm for MZx was deduced from the broadening of the $(\bar{1}\,1\,1)$ peak. That peaks corresponding to $2\theta = 30.32°$ (relative intensity is 100), 35.20° (19), 42.84° (3), 50.56° (45), 60.04° (29), 63.00° (8), 74.52° (6) are developed in the XRD pattern of TZ50 (Fig. 1) makes it similar to the standard pattern of cubic ZrO_2 (JCPDS No. 27-997). From the FWHM of the (1 1 1) peaks, grain size of 7.6 nm for TZ50 was calculated. The specific surface areas of TZ50 and MZ96 determined by BET method (S_{BET}) as well as calculated from the XRD results (S_{XRD}) are listed in Table 1. As XRD-derived surface area is based on the assumption that the primary particle is monodispersed, the coincidence between S_{BET} and S_{XRD} for TZ50 shows that it has rare agglomeration. In fact its TEM picture (not shown here) also confirms that. Comparing the surface area values in Table 1, one may conclude that the degree of agglomeration in MZ96 is much heavier than that in TZ50. The TEM observation (Fig. 2) clearly shows that MZ96 forms cubic agglomerate dimensioned ca. 100 nm, which is composed of primary grain ca. 10 nm.

The identification of tetragonal ZrO_2 or cubic ZrO_2 with poor crystallinity by XRD technique is precluded by peak broadening. As Raman spectroscopy can be successfully employed to identify the non-monoclinic phase of zirconia, we also resorted to LRS. That only six Raman active modes appear in the Raman spectrum of TZ50 (Fig. 3)

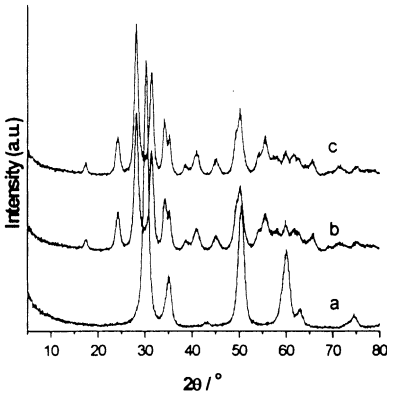

Fig. 1. XRD patterns of (a) TZ50, (b) MZ50 and (c) MZ96.

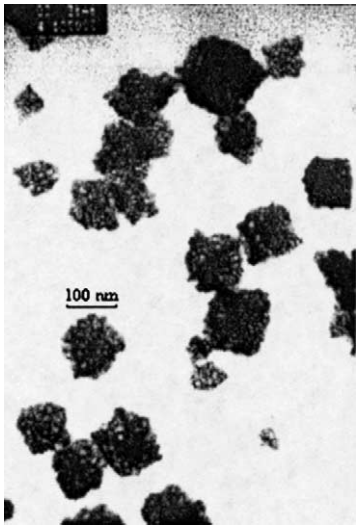

Fig. 2. TEM picture of MZ96.

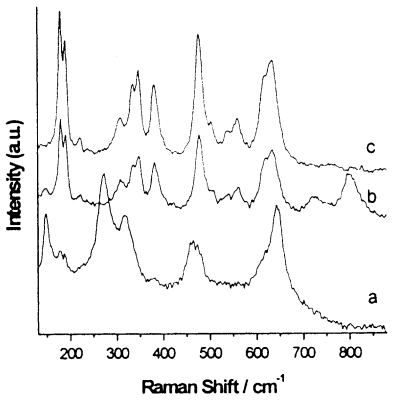

Fig. 3. Raman spectra of (a) TZ50, (b) MZ50 and (c) MZ96.

clearly confirms that its crystal phase is tetragonal [16]. Additional three bands around 150, 725 and 795 cm^{-1}, other than the rest bands characteristic of MZ, are developed only in the Raman spectrum of MZ50, but not in the spectrum of MZ96 (Fig. 3). The band at 150 cm^{-1} belongs to TZ and the band at 725 cm^{-1} to MZ [17], but we don't know the assignment of the band at 795 cm^{-1} at present. Considering LRS is more sensitive than XRD to the solid surface, the appearance of band at 150 cm^{-1} indicates that there exist some TZ regions on the surface of MZ50. Refluxing the hydrous zirconia longer made MZ96 a pure MZ examined both by XRD and by LRS. Connecting the LRS-derived tetragonal phase with the XRD-indicated cubic-like phase for TZ50, one may agree that its crystal phase is a slightly distorted tetragonal phase. This distorted tetragonal phase may be derived from the nanosized primary particle. As EXAFS measurements [18] have showed that the mean coordination number of Zr is reduced in nanocrystalline ZrO_2 ($D = 30$ nm) compared to powders with much larger particles ($D = 1000$ nm), a slight distortion from ideal tetragonal structure in our nanosructured TZ50 sample ($D = 7.6$ nm) is reasonable.

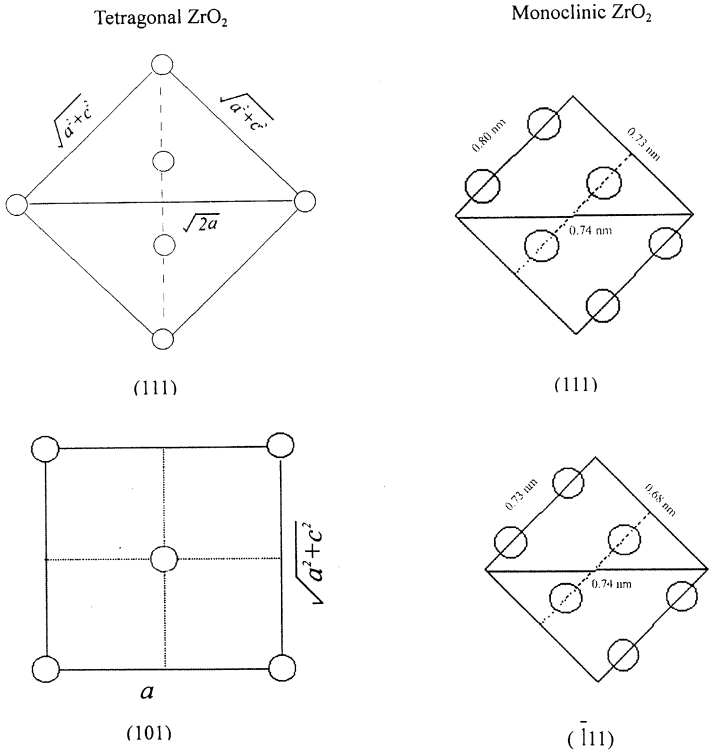

Fig. 4. Zr^{4+} array in different planes of tetragonal and monoclinic (JCPDS No.37-1484) ZrO_2.

For the crystal phases of TZ50 and MZ96, especially in the surface, are tetragonal and monoclinic, the following analysis is confined to these two samples.

3.2. Zr^{4+} density in different planes

Calculations based on density functional theory (DFT) method with adopting the Teufer's lattice constants for tetragonal ZrO_2 (JCPDS No. 42-1164) show that the surface energy of (1 0 1) plane is the lowest for pure TZ [19]. Using HRTEM, Morterra et al. [20] observed that the (1 1 1) plane is preferentially exposed for Y-doped TZ calcined at temperature lower than 873 K, while the (1 0 1) plane is frequently observed at high calcination temperature. For undoped MZ calcinated at 873 K the (1 1 1) and ($\bar{1}$ 1 1) planes are most frequently seen [20]. Thus the following analysis about Zr^{4+} density is based on these findings: (1 1 1) and (1 0 1) planes for TZ, (1 1 1) and ($\bar{1}$ 1 1) planes for MZ are generally the preferential planes.

From the crystal structure of zirconia one can draw out the (1 1 1) and (1 0 1) planes of TZ as well as (1 1 1) and ($\bar{1}$ 1 1) planes of MZ (Fig. 4), for simplicity all the O^{2-} ions are omitted. The lattice parameters of MZ can be unambiguously obtained from JCPDS No.37-1484 for the XRD pattern of MZ96 sample is entirely in accord with the standard file. Unfortunately the cubic-like bulk phase and the tetragonal-like surface phase of TZ50 sample make the selection of lattice constants for calculating the surface Zr^{4+} density of TZ is uncertain. So several serial lattice parameters were adopted here to calculate the surface Zr^{4+} density of TZ. The results are listed in Table 2.

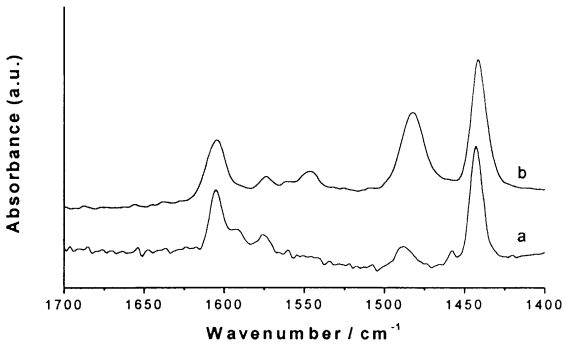

Fig. 5. IR spectra after pyridine adsorption of (a) TZ50 and (b) MZ96.

3.3. Surface acidic features of zirconia

The identification of the acid type can be achieved from IR spectra after pyridine adsorption (Py-IR), for pyridium ion (formed at B acid sites) displays 1540 cm^{-1} band and coordinately bonded pyridine (formed at L acid sites) gives 1445 cm^{-1} band [21]. On the monoclinic MZ96 sample there exists both Brønsted acid sites and Lewis acid sites, while on the tetragonal TZ50 only type L acid sites can be detected by IR measurement after pyridine adsorption (Fig. 5). This is just opposite to Li's result [10] in the case of TZ. They reported almost only B acid sites exist on TZ. As a matter of fact, Li et al. performed their experiments in air atmosphere for convenience. Maybe some unknown species adsorbed on their samples make the appearance of the pyridium ion band.

The lack of precise ε for 1540 cm^{-1} and 1445 cm^{-1} bands hampers the accurate calculation of the acid-site density by IR technique. In such case, we intend to base such analysis on Andersen's results. By combining the IR and gravimetric mea-

Table 2
Zr^{4+} densities on different planes of monoclinic and tetragonal ZrO_2

	Monoclinic		Tetragonal					
	(1 1 1)	($\bar{1}$ 1 1)	(1 1 1)	(1 0 1)	(1 1 1)	(1 0 1)	(1 1 1)	(1 0 1)
Zr^{4+} density (nm^{-2})	8.1	9.0	10.0	8.6	6.5	5.3	6.6	5.4
Adopted lattice parameters (nm)	$a = 0.531$, $b = 0.521$, $c = 0.515$ $\beta = 99.22°$		$a = 0.364$ $c = 0.527$		$a = 0.512$ $c = 0.525$		$a = 0.509$ $c = 0.518$	
JCPDS No.	37-1484		42-1164		17-923		14-534	

Table 3
Surface acid-site densities of TZ50 and MZ96 samples

Sample	Surface acid-site density (nm^{-2})		
	n_B[a]	$n_B + n_L$[b]	n_c[c]
TZ50	–	1.7	1.7
MZ96	0.5	3.8	3.4

[a] The density of Brønsted acid sites calculated from IR data.
[b] The density of total acid sites calculated from IR data.
[c] The density of total acid sites determined by NH_3-adsorption measurements.

surements, Anderson et al. [15] obtained these values for their silica-zirconia samples with ZrO_2 content varied from 9 to 75 mol%. The ε values of 1540 and 1445 cm^{-1} bands for pure ZrO_2 were deduced by linear extrapolating Anderson's data as $\varepsilon_L = 1.62$ cm μmol^{-1} and $\varepsilon_B = 1.19$ cm μmol^{-1}. Thus the surface acid-site densities of TZ50 and MZ96 were calculated according to Eq. (1) and listed in Table 3.

The total acid-site densities of our samples derived from IR data is considerably greater than Tanabe's results [22], about 0.02 nm^{-2}, determined by the same method except that they used their unpublished ε values. The acceptable coincidence of our acid-site values obtained by IR and NH_3-adsorption measurements may show that the ε values adopted here are correct as a whole (Table 3). Our irreversible NH_3 adsorption amount on ZrO_2 is comparable with literature's value [23], 3 NH_3/nm^2. Although the present values about 1.7 NH_3/nm^2 adsorbed on TZ and 3.4 NH_3/nm^2 on MZ are higher than Hertl's report [24], 0.45 NH_3/nm^2 and 0.7 NH_3/nm^2, respectively (measured at 423 K, 30 K higher than our used), the tendency that more acid sites exist on monoclinic ZrO_2 is consistent. The temperature difference may be a good reason for the difference of NH_3 adsorption amount between Hertl's results and ours.

With the aim of relating the Zr^{4+} density to the surface acid-site density for nanostructured ZrO_2 in mind, we plotted the concerned data in Fig. 6. There exists a parallel relationship between Zr^{4+} density and the acid-site density for TZ and MZ except that the Zr^{4+} density calculated from JCPDS No. 42-1164, which was determined at 1523 K by Teufer. It's apprehensible that there is an obvious difference of lattice constants for TZ

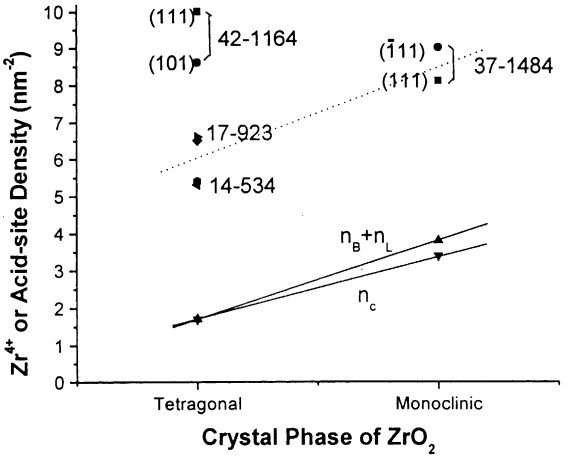

Fig. 6. Zr^{4+} density and acid-site density of tetragonal and monoclinic ZrO_2. The texts on the left of points are the Miller indexes, the right-side text the JCPDS No, $n_B + n_L$ the density of total acid sites calculated from IR data, n_C the density of total acid sites determined by NH_3-adsorption measurements.

between Teufer's ZrO_2 and ZrO_2 calcined at moderate temperature. In 1990, Kutty et al. [25] reported the cell parameters for their TZ, prepared by hydrothermal method at 473 K without any further calcination, are $a = 0.513$ nm and $b = 0.516$ nm. Similar values, $a = 0.514$ nm and $b = 0.517$ nm, have been determined for TZ calcinated at 713 K [26]. The Zr^{4+} density in (1 1 1) and (1 0 1) planes of TZ derived from these two serial lattice parameters, about 6 Zr^{4+}/nm^{-2}, is in the middle of those values calculated from JCPDS No. 17-923 and 14-534 (Fig. 6). So the surface Zr^{4+} densities of TZ and MZ derived from their preferential planes (about 6 Zr^{4+}/nm^{-2} and 8–9 Zr^4/nm^{-2}, respectively), are approximately 3 times their surface acid-site densities determined by NH_3-adsorption measurements (1.7 nm^{-2} and 3.4 nm^{-2}, respectively).

Acknowledgements

Authors are gratefully acknowledged for the supports of Scientific Key Foundation under Ministry of Education (grant No. 99018), the Research Fund for the Doctoral Program of Higher Education (grant No. 200000-5520) and the Natural Science Foundation (grant No. 200003006).

References

[1] K. Tanabe, Mater. Chem. Phys. 13 (1985) 347.
[2] T. Yamaguchi, Catal. Today 20 (1994) 199.
[3] P.D.L. Mercera, V.J.G. Ommen, E.B.M. Doesburg, A.J. Burggraat, J.R.H. Ross, Appl. Catal. 57 (1990) 127; Appl. Catal. 71 (1991) 363.
[4] S. Damyanova, P. Grange, B. Delmon, J. Catal. 168 (1997) 421.
[5] A. Khodakov, B. Olthof, A.T. Bell, E. Iglesia, J. Catal. 181 (1999) 205.
[6] V.A. Tsipoutiati, A.M. Efstathiou, Z.L. Zhang, X.E. Verykios, Catal. Today 21 (1994) 579.
[7] S.K. Maity, M.S. Rana, B.N. Srinivas, S.K. Bej, M.G. Dhar, P.T.S.R. Rao, J. Mol. Catal. A 153 (2000) 121.
[8] Sh. Xie, E. Iglesia, A.T. Bell, Chem. Mater. 12 (2000) 2442.
[9] G.K. Chuah, S.H. Liu, S. Jaenicke, J. Li, Micopor. Mesopor. Mater. 39 (2000) 381.
[10] W. Li, Y. Yin, R. Gao, R. Hou, J. Mol. Catal. (China) 13 (1999) 186.
[11] J.C. Yori, J.M. Parera, Catal. Lett. 65 (2000) 205.
[12] W. Stichert, F. Schüth, S. Kuba, H. Knözinger, J. Catal. 198 (2001) 277.
[13] Y. Zhao, Y. Zeng, K. Tao, Chinese J. Catal. 23 (2002) 168.
[14] K.-H. Jacob, E. Knözinger, S. Benfer, J. Mater. Chem. 3 (1993) 651.
[15] J.A. Anderson, C. Fergusson, I. Rodriguez-Ramos, A. Guerrero-Ruiz, J. Catal. 192 (2000) 344.
[16] D. Michel, M. Perez, Y. Jorba, R. Collongues, J. Raman Spectrosc. 5 (1976) 163.
[17] T. Hirata, E. Asari, A. Kitajima, J. Solid State Chem. 110 (1994) 201.
[18] R. Nitsche, M. Winterer, M. Croft, H. Hahn, Nucl. Instrum. Methods B 97 (1995) 127.
[19] F. Haase, J. Sauer, J. Am. Chem. Soc. 120 (1998) 13503.
[20] C. Morterra, G. Cerrato, L. Ferroni, L. Montanaro, Mater, Chem. Phys. 37 (1994) 243.
[21] E.P. Parry, J. Catal. 2 (1963) 371.
[22] Y. Nakano, T. lizuka, H. Hattori, K. Tanabe, J. Catal. 57 (1979) 1.
[23] A. Gervasini, A. Auroux, J. Catal. 131 (1991) 190.
[24] W. Hertl, Langmuir 5 (1989) 96.
[25] T.R.N. Kutty, R. Vivekanandan, S. Philip, J. Mater. Sci. 25 (1990) 3649.
[26] Y. Zeng, Ph.D. Thesis, Nanjing University, Nanjing, 1994.